Microvasculopathy in SMA is driven by a reversible autonomous endothelial cell defect

Microvasculopathy in SMA is driven by a reversible autonomous endothelial cell defect

Haiyan Zhou[1,2#]*, Ying Hong[3#], Mariacristina Scoto[4#], Alison Thomson[5 #], Emma Pead[6#], Tom MacGillivray[6], Elena Hernandez-Gerez[5], Francesco Catapano[4], Jinhong Meng[1], Qiang Zhang[1], Gillian Hunter[7§], Hannah K. Shorrock[7¶], Thomas Ng[7], Abedallah Hamida[5], Mathilde Sanson[4], Giovanni Baranello[4], Kevin Howell[8], Thomas H. Gillingwater[7], Paul Brogan[3], Dorothy A. Thompson[9]*, Simon H. Parson[5]* and Francesco Muntoni[2,4]*

1. Genetics and Genomic Medicine Research and Teaching Department, Great Ormond Street Institute of Child Health, University College London, London, UK

2. NIHR Great Ormond Street Hospital Biomedical Research Centre, Great Ormond Street Institute of Child Health, University College London, London, UK

3. Infection, Inflammation and Rheumatology Section, Great Ormond Street Institute of Child Health, University College London, London, UK

4. The Dubowitz Neuromuscular Centre, Developmental Neurosciences Research and Teaching Department, Great Ormond Street Institute of Child Health, University College London, London, UK

5. Institute of Medical Sciences, University of Aberdeen, Foresterhill, Aberdeen, UK

6. Centre for Clinical Brain Sciences, University of Edinburgh, Edinburgh, UK

7. Edinburgh Medical School, Biomedical Sciences, College of Medicine & Veterinary Medicine, University of Edinburgh, Edinburgh, UK

8. Microvascular Diagnostics, Institute of Immunity and Transplantation, University College London, London, UK

9. Tony Kriss Visual Electrophysiology Unit, Clinical and Academic Department of Ophthalmology, Sight and Sound Centre, Great Ormond Street Hospital, London, UK

[#] Shared first authorship

* Shared corresponding authorship

¶ Current address: The RNA Institute, University at Albany, State University of New York, Albany, USA

§ Current address: Biological and Biomedical Sciences, Glasgow Caledonian University, Glasgow, UK

Address correspondence to:

Haiyan Zhou, Great Ormond Street Institute of Child Health, University College London, 30 Guilford Street, London, WC1N 1EH, United Kingdom. Phone: +44 (0) 207 905 2868; Email: haiyan.zhou@ucl.ac.uk.

Dorothy A. Thompson, Tony Kriss Visual Electrophysiology Unit, Clinical and Academic Department of Ophthalmology, Sight and Sound Centre, Great Ormond Street Hospital for Children, 40-41 Queen Square, London, WN1N 3AJ, United Kingdom. Phone: +44 (0) 207 405 9200 7505; Email: dorothy.thompson@ucl.ac.uk.

Simon H. Parson, Institute of Medical Sciences, University of Aberdeen, Foresterhill, Aberdeen, AB25 2ZD, United Kingdom. Phone: +44 (0) 122 427 4328; Email: simon.parson@ucl.ac.uk.

Francesco Muntoni, Great Ormond Street Institute of Child Health, University College London, 30 Guilford Street, London, WC1N 1EH, United Kingdom. Phone: +44 (0) 207 905 2111; Email: f.muntoni@ucl.ac.uk.

Conflict of interest statement

Professor Francesco Muntoni has served on scientific advisory boards for Sarepta, Pfizer, Roche, Novartis, Biogen, and Dyne Therapeutics, his institute receives research support from Biogen and Sarepta, and has received funding for trials from Novartis, Biogen, Genethon, Pfizer, Roche, and Sarepta Therapeutics. Dr Mariacristina Scoto has served on scientific advisory boards for Roche, Biogen and Novartis and has received funding for trials from Roche and Biogen. Dr Giovanni Baranello has received speaker and consulting fees from Biogen, Novartis and Roche, grant support and SMA studies sponsored by Novartis and Roche. Professor Paul Brogan has received consultancy fees from SOBI, Novartis, and Roche. Professor Thomas H. Gillingwater has served on global scientific and clinical advisory boards for SMA Europe and Roche. All the other authors declare no conflicts of interest in this study.

Abstract

Spinal muscular atrophy (SMA) is a neuromuscular disorder due to degeneration of spinal cord motor neurons caused by the deficiency of the ubiquitously expressed SMN protein. Here, we present a retinal vascular defect in patients, recapitulated in SMA transgenic mice, driven by failure of angiogenesis and maturation of blood vessels. Importantly, the retinal vascular phenotype was rescued by early, systemic SMN restoration therapy in SMA mice. We also demonstrate in patients an unfavourable imbalance between endothelial injury and repair, as indicated by increased circulating endothelial cell counts and decreased endothelial progenitor cell counts in blood circulation. The cellular markers of endothelial injury were associated with disease severity and improved following SMN restoration treatment in cultured endothelial cells from patients. Finally, we demonstrated autonomous defects in angiogenesis and blood vessel formation, secondary to SMN deficiency in cultured human and mouse endothelial cells, as the underlying cellular mechanism of microvascular pathology. Our cellular and vascular biomarkers findings indicate microvasculopathy as a fundamental feature of SMA. Our findings provide mechanistic insights into previously described SMA microvascular complications, and highlight the functional role of SMN in the periphery, including the vascular system, where deficiency of SMN can be addressed by systemic SMN-restoring treatment.

Introduction

Spinal muscular atrophy (SMA) is an autosomal recessive neuromuscular disorder caused, in ~95% of patients, by homozygous deletion of the *Survival Motor Neuron 1* gene (*SMN1*) (1). The neuropathological hallmark of SMA is the selective degeneration of lower motor neurons, with ensuing muscle atrophy and weakness. In the most common and severe form (Type 1 SMA, or Werdnig Hoffman disease), children die within the first 2 years of life, without acquiring the ability to sit. Relatively milder forms are intermediate or Type 2 SMA, in which children sit but are unable to walk; and Type 3 SMA, in which ambulation is acquired although often lost with age (2). SMA Type 1 is the most common genetic cause of infant mortality, with an incidence of around 1:6000 live births and a carrier frequency of ~1:35 in the Caucasian population (3).

Notable breakthroughs in therapy for SMA have recently been achieved using therapeutic interventions aimed at increasing SMN protein levels (4). Nusinersen is an antisense oligonucleotide (AON) drug that has been approved by the US Food and Drug Administration (FDA) and European Medicines Agency (EMA), for the treatment of patients with SMA (5, 6). It increases full-length SMN protein expression by targeting the intronic splicing silencer N1 element (ISS-N1) in intron 7 of the *SMN2* gene and augmenting exon 7 inclusion in the mature *SMN2* mRNA (7, 8). Nusinersen is delivered exclusively to the central nervous system (CNS) by regular intrathecal injections. *SMN1* gene replacement therapy using adeno-associated viral vectors (AAV) is another effective therapy for SMA (9-11). Onasemnogene abeparvovec (AVXS-101,) an AAV9-SMN gene therapy drug approved by FDA and EMA, is a one-off treatment delivered intravenously in infants with SMA Type 1, and is able to cross the blood-brain barrier. The orally bioavailable small molecules *SMN2* splice modulators risdiplam and branaplam are also effective, with risdiplam having been approved by FDA and EMA (12, 13). In contrast to nusinersen, which acts exclusively in the

CNS, both onasemnogene abeparvovec and risdiplam are delivered systemically and therefore address SMN deficiency in both the CNS and peripheral organs (14), although differences in peripheral biodistribution between these two therapies exist.

The SMN protein is ubiquitously expressed. While SMA is primarily a lower motor neuron disease, an increasing body of evidence from clinical and animal-based studies indicates a contribution of peripheral organs to the complex pathogenesis of the disease (15-17). It is therefore important to determine which organs have a clinically relevant requirement for SMN protein, as different therapies may differentially address the SMN deficiency in discrete tissues and organs.

Vascular-related defects have been reported in severe cases of infantile SMA, and in mouse models of SMN deficiency. These include digital necrosis, distal vascular thrombosis and skin necrosis (18-20); tail and ear necrosis, decreased density of capillaries in spinal cord and intestine in SMA mice (21-23); and decreased density of capillaries in skeletal muscle from both patients and mice (22,24). Cardiovascular abnormalities, including congenital heart disease and heart failure, have also been reported in severe SMA patients and SMA mice (19, 25-27). These defects result in widespread tissue hypoxia in animal models of SMA, to which motor neurons appear to be particularly susceptible (28). In addition, changes in the expression of some vascular-related factors have been reported in blood samples of patients with SMA, suggesting that the vascular abnormalities could be pervasive in the SMA patient population (29).

Given the essential nature of the blood supply to the spinal cord and brain, and the sensitivity of motor neurons to defects in oxygen supply from disordered capillary networks, it is important to clarify the nature of a microvascular disease phenotype in SMA. Here, we used paediatric retinal imaging to reveal defects in retinal vascularisation in SMA patients. We

recapitulated the phenotype in mouse models of severe SMA and demonstrated defective angiogenesis and maturation of the primary retinal vasculature. In addition, we show that antisense therapy, delivered systemically at birth to increase SMN protein expression, can normalise the microvascular defect in these mice. Using blood samples from patients, we go on to show increased vascular damage and decreased vascular repair. Importantly, this vascular damage was correlated with disease severity and *SMN2* copy number. Finally, using two different cellular systems, we show that the vascular defect is driven by a cell-autonomous defect in the ability of SMN-depleted endothelial cells to form vessels.

Results

A retinal vascular phenotype in SMA patients

Retinal imaging is a reliable indicator of vascular health and disease in the CNS (30). Conventional colour fundus photography captures a field of view of 30-45°, but here we used ultra-widefield imaging to capture an extended image of the retinal vasculature, with an angular field of view of up to 200°. This allowed us to assess larger areas of the retina, but as the imaging equipment requires postural cooperation from participants to position the eye at the optimal distance for focus and field of view, we restricted our study to SMA Type 2 and 3 patients (31). The patients had normal visual acuity and did not complain of any visual difficulty.

We analysed ultra-widefield images from 21 eyes of 11 SMA patients (images from one eye were excluded due to poor view of the vasculature obstructed by eyelash) and 46 eyes of 23 healthy control children, to generate Fractal Dimension (FD) measures of retinal vessel branching complexity. FD is a unitless index of the degree of complexity and hence space filling by the vessels, on the retinal surface. FD is a well-established parameter for objectively characterising the complexity of the retinal microvasculature (32) and is used in neurogenerative diseases as a surrogate for cerebral microvasculature changes (31). FD values generally range between 1 and 2, and we considered a change of 0.01 to be biologically relevant based upon our previous experience (Pead E, unpublished observations). A lower FD value indicates a pattern of retinal vessels that is less space filling, analogous to increased lacunarity or mesh size. We calculated the FD in three regions of interest (ROI); a *Standardised* ROI for ultra-wide field images (VAMPIRE-UWF), further subdivided into a *Posterior* ROI (centred around the optic disc) and a *Midperipheral* ROI (the difference in area between the standardised and posterior ROI) (see Methods). SMA patients had a

significantly lower FD in the *Standardised* ROI using two different methods of segmentation (β = -0.019, P< 0.001 by the Pellegrini method; β = -0.017, P= 0.001 by the IterNet method; Table 1) (33, 34), indicating that the vascular patterning was less space filling within this ROI (Figure 1). Using the IterNet method of segmentation that detects smaller branching vessels (33), SMA patients exhibited a significantly lower FD in the Posterior ROI compared to controls (β = -0.018, P< 0.001) (Figure 1). The mean FD was lower in the midperiphery zone but did not reach statistical significance.

The significant difference in FD indicates a less dense and less complex primary retinal vasculature in SMA patients when compared to age matched control children.

Demonstration of the retinal vascular phenotype in SMA mice

In order to further investigate this retinal vascular phenotype, we explored the possibility that the primary retinal vasculature defect could be replicated in the 'Taiwanese' mouse model of severe SMA (35). In mice, the retinal vasculature develops exclusively postnatally, and can be demonstrated by immunohistochemical staining of whole mount retinae, using a vascular endothelial cell marker Griffonia Simplicifolia Lectin I/ isolectin B4 (GSL I/ IB4). Stained retinas showed that vascular defects were readily apparent in the SMA mice from a pre-symptomatic age: postnatal day 3 (P3). In the SMA retinas the centripetal pattern of angiogenic outgrowth from the optic disc toward the periphery lagged behind the retinas of unaffected control littermates (Figure 2A). AngioTool software (36), which allows for semi-automated reconstruction and quantification of vascular networks, was used to analyse the morphometric and spatial parameters of the retinal vasculature. A dramatic disease phenotype was apparent in all parameters of vascular network outgrowth complexity measured. Vessel outgrowth, a measure of overall microvascular density, and expressed as a percentage of total retinal area, was significantly reduced in SMA compared to control mice at early

symptomatic P5 (Control: 57.1±2.3% and SMA: 32.0±2.2%, P<0.001), and late symptomatic P8 (Control: 78.2±2.0% and SMA: 27.6±2.0%, P<0.001), but not at pre-symptomatic P3 (Control: 34.1±0.8% and SMA: 28.8±2.8%, P=NS) (Figure 2B) time points. Vessel outgrowth increased in control retinas between P3 and P5, and between P3 and P8 (P<0.001), but not in SMA retinas over the same periods. Numbers of microvessel endpoints, a measure of the number of likely angiogenic 'tips', was significantly reduced in SMA compared to control retinas at P3 (Control: 155.7±8.0 and SMA: 96.2±4.5, P<0.001), P5 (Control: 233.4±10.4 and SMA: 93.5±6.8, P<0.001) and P8 (Control: 301.3±11.9 and SMA: 84.9±6.2, P<0.001) (Figure 2C). Numbers of endpoints increased in control retinas between P3 and P5, and between P3 and P8 (P<0.001), but not in SMA retinas over the same periods. The decreases in microvascular outgrowth and vessel endpoints in SMA retinas indicate decreased angiogenesis and were inversely correlated with a significant increase in lacunarity (a measure of network mesh size) in SMA at P3 (Control: 0.87±0.06 and SMA: 1.72 ±0.11, P<0.001), P5 (Control: 0.22±0.04 and SMA: 0.71±0.05, P<0.001) and P8 (Control: 0.2±0.01 and SMA: 0.91±0.12, P<0.001) (Figure 2D). Lacunarity decreased in control and SMA retinas between P3 and P5 (P<0.001), and between P5 and P8 (P<0.001), indicating a developing and increased complexity of the microvascular plexus, resulting in a highly branched and ramified structure in control, but not in SMA retinas. Together these data support the patient data and reveal reduced vessel complexity (FD in the patients) in the retina as a consistent and potentially important phenotype in SMA.

Preparations in which blood vessels were labelled by GSL I/ IB4, also show a population of small, isolated cells. GSL I/IB4 is an established marker of activated and quiescent microglia (37). The morphology of blood vessels and microglia are sufficiently different to make their identification possible, and this showed that there was an apparent increase in the number of

microglia present in SMA retinas, especially in the periphery, where no blood vessels are present (Figure 2A).

Detailed investigation of the retinal vasculature in SMA mice showed that the naked collagen IV basal lamina tubes, indicative of vessel loss, were not present in either SMA or control mice retinas, rather vessel and basal lamina were closely correlated (Figure 2E). This suggests that there was no evidence of the vessel regression, which would be indicative of a degenerative phenotype. Further, those vessels present in SMA retinas were failing to mature into arterioles, indicated by a lack of acquisition of smooth muscle (stained with α-smooth muscle actin) into vessel walls when compared with the mature, differentiated arterioles in control retinas (Figure 2F). Finally, the pre-existing astrocytic base (stained with glial fibrillary acidic protein), over which developing retinal vessels grow, appeared similar in control and SMA mice. However, the alignment of vessels upon this framework was very weak in SMA animals (Figure 2G). These findings are consistent with an impaired angiogenic phenotype in SMA mice. Interestingly, the pre-existing, embryonic, hyaloid vasculature appeared near normal in P5 SMA mice compared to control retinas (Supplemental Figure 1).

Taken together, these data reveal an important microvascular pathology of the retina in the SMA mice, likely related to SMN protein deficiency. This phenotype, present in both SMA patients and mouse models, points toward fundamental defects in angiogenesis and microvascular development in the vessels supplying the CNS in SMA.

Systemic *in vivo* antisense oligonucleotide treatment restores the retinal vascular network

To determine if these microvascular pathologies are amendable to therapeutic intervention, we next studied the outcome of the administration of a 25mer morpholino therapeutic AON

(PMO25), on SMA mouse retinas. SMA mice were treated with a single subcutaneous injection of PMO25 at 40 μg/g at P0 as described previously (21, 38). At a late symptomatic timepoint of P10, retinas were collected from saline-treated SMA mice, PMO25-treated SMA mice and healthy littermate controls. Quantitative real-time PCR on *SMN2* transcripts in mouse retinas showed significant increase by 5.5-fold in the full-length *SMN2* transcripts ($P<0.0001$) and decease by 37% in the *SMN2* transcripts lacking exon 7 (Δ7 SMN2) ($P=0.0005$) in PMO25-treated SMA mice compared to untreated SMA controls (Figure 3A), suggesting the high efficacy of PMO25 in augmenting *SMN2* exon7 splicing. The therapeutic effect of PMO25 was further confirmed by western blotting, with over 8-fold increase of SMN protein after PMO25 treatment (Figure 3B). Immunohistochemical staining of the retinal vasculature using GSL I/IB4, showed the expected, severe pathology in the SMA retinas, but also the recovery of vascularity in the PMO25-treated SMA mice (Figure 3C). This was reflected in the restoration of key parameters of network complexity at P10. Vessel outgrowth, expressed as a percentage of total area, was significantly decreased in SMA compared to healthy control mice (Control: 95.7±0.33%, SMA: 34.2±1.7%, $P<0.001$), and significantly restored following PMO25 treatment (SMA+PMO25: 82.9±0.35%, $P<0.001$). Numbers of endpoints were significantly decreased in SMA compared to control mice (Control: 710±42.9, SMA: 203±37.9, $P<0.05$), and almost completely restored after PMO25 treatment (SMA+PMO25: 559.8±133.6, $P<0.05$). Finally, the significantly increased lacunarity observed in the SMA compared to control mice (Control: 0.21±0.01, SMA: 2.81±0.47, $P<0.001$), was also ameliorated after PMO25 treatment (SMA+PMO25: 0.31±0.04, $P<0.001$) (Figure 3C, D).

These data support the idea that pathology of blood vessels, and constituent endothelial cells in SMA, which lie on the systemic, vascular face of the blood-brain and blood-retinal barriers, is reversible and amendable to systemically delivered SMN-restoring AON.

Reduced retinal vascularity precedes a reduction in neuronal population and increased microgliosis in SMA mice

In order to determine whether the severe defects in vascularisation were associated with any damage to, or loss of, neuronal population of the retina, we visualised and quantified the neural retina in SMA mice. The neural retina is a deep, multi-layered structure. Initial quantification of hematoxylin and eosin (H&E) stained sections of whole retinas from SMA mice at P5 and P8 (Figure 4A), showed a significant reduction in retinal thickness in SMA retinas compared to controls at P5 (Control: 162.8±5.8µm and SMA: 138.2±1.3µm, $P<0.01$) and P8 (Control: 132.8±3.1µm and SMA: 89.0±3.0µm, $P<0.001$) (Figure 4B). Note that retinal thickness decreased in both control and SMA retinas between P5 and P8 ($P<0.001$, Figure 4B). A further detailed immunohistochemical analysis of the different cells which make up the multi-layered retina, showed that numbers of retinal ganglion cells (RGCs) identified by BRN3a staining (Figure 4C), were similar at P5 in SMA and control littermate mice (Control: 4.44±0.4 and SMA: 4.77±0.3, P=NS), but significantly reduced in SMA at P8 (Control: 3.7±0.2 and SMA: 1.9±0.2, $P<0.001$) (Figure 4D). There was no change in numbers of RGCs in control retinas between P5 and P8 (P=NS), while SMA retinas showed a significant loss of RGCs over the same period ($P<0.001$, Figure 4D). Next, and focussing on P8, we stained amacrine and horizontal cells with Pax6 (Figure 4E), which revealed a significant reduction in SMA retinas compared to healthy littermate controls (Control: 21.4±0.9 and SMA: 9.6±1.1, $P<0.0001$, Figure 4F).

Microglia are implicated in both vessel and synaptic remodelling as well as in disease processes in the retina (39), and we had seen their apparent increase in SMA mouse retinas in our original observations (Figure 2A). We therefore quantified the microglia in wholemount preparations, stained with GSL I/ IB4 lectin and identified by their morphology (Figure 4G). Numbers of microglia were not changed in SMA retinas at P3 compared to control littermates

(Control: 13.0±1.07 and SMA: 19.8±1.7, P=NS) but significantly increased at P5 (Control: 10.9±1.2 and SMA: 19.7±1.9, P<0.05) (Figure 4H). By P8 microglia were almost absent in control retinas but were dense in SMA retinas (Control: 2.0±0.9 and SMA: 32.8±3.7, P<0.001, Figure 4H). Over this period numbers of microglia were consistent between P3 and P5 in control retinas (P=NS) but decreased between P5 and P8 (P<0.05). In SMA retinas, microglia were again stable between P3 and P5 (P=NS) but increased between P5 and P8 (P<0.001, Figure 4H). We also confirmed the identity of these cells using a second established marker, ionized calcium binding adaptor molecule 1 (iba1) (40). This showed the same pattern of increases in microglia in SMA at P8, with the appearance of large numbers of microglia in the deeper synaptic inner and outer nuclear layers in sections of the retina (Supplemental Figure 2). Conversely, in control retinas, microglia were noticeable by their absence in these deeper layers.

Finally, we examined the light sensitive photoreceptors of the retina, where we identified rods by red/ green and blue opsin staining, and cones identified by rhodopsin staining at P8 (Figure 4I). Photoreceptors were depleted in SMA retinas compared to control littermates (Control rods: 8.1±0.6% and SMA: 0.9±0.3%, P<0.001; Control Cones: 23.4±2.5% and SMA: 9.2±3.1%, P<0.01, Figure 4J).

The loss of these retinal cells likely underlies the dramatic thinning of the retina which we initially observed in Figure 4A. These data show a close association between an early reduction in CNS vascularity and a concurrent or later loss of neurons. In turn this is associated with a progressive increase in microglia.

Endothelial injury markers are increased in peripheral blood from SMA patients

To gather further insight on the microvascular system, we investigated the markers of endothelial injury in blood circulation in SMA patients. Vascular health is determined by a

balance between endothelial injury and repair (41-43). In response to chronic vascular inflammation or trauma associated with endothelial injury, endothelial cells detach from vessel walls and enter the blood circulation (44-46). These circulating endothelial cells (CECs) allow vascular injury to be tracked in patients with vasculopathy (47-49).

Therefore, to assess whether vascular damage was present in patients with SMA, the levels of CECs in peripheral blood were measured and compared with age-matched healthy controls. The CEC count in patients with SMA (n=32) was higher at 147/mL (8-800) compared to 15/mL (0-64) in healthy controls (n=67, $P< 0.0001$) (Figure 5A). Significant differences in the CEC count were also detected in SMA patients with differing clinical severity when compared to healthy controls: Type 1 SMA patients 291/mL (144-640, n=6, $P<0.0001$); Type 2 patients 169/mL (8-800, n=12, $P< 0.0001$); and Type 3 patients 64/mL (8-176, n=11, $P=0.3111$). Significant difference was also detected between SMA Type 1 and Type 3 patients ($P<0.0001$) (Figure 5B). Moreover, a significant negative correlation was found between the CEC count and *SMN2* copy number ($r^2 = 0.2344$, $P< 0.05$) (Figure 5C).

These results provide evidence of an ongoing endothelial injury in SMA patients and suggest a close association between endothelial injury and disease severity and/or *SMN2* copy number. These findings also highlight the potential utility of CEC counts in peripheral blood as a novel cellular biomarker for SMA-associated vasculopathy.

The potential of endothelial repair is decreased in SMA patients

In the presence of vascular damage, concurrent recruitment of bone marrow-derived endothelial progenitor cells (EPCs) is an important mechanism for ongoing endothelial repair (43, 50). To assess this in SMA patients, we next carried out colony-forming unit (CFU) assays in angiogenic medium, a specific enumeration system for EPCs (51). We found a significant decrease in the number of CFUs from EPCs isolated from SMA patient blood

samples (8 CFUs/well, range: 1-27, n=28), compared to age-matched healthy control (19 CFUs/well, range: 8-40, n=13; P= 0.0002) (Figure 5D). There was, however, no significant difference in the EPC-CFU count between different SMA subtypes: the reduction in EPC-CFU was similar between SMA Type 1 (6 CFUs/well, range: 0-17, n=7), Type 2 (6 CFUs/well, range: 1-12, n=11) and Type 3 patients (9 CFUs/well, range: 3-27, n=8) (Figure 5E). Further, no correlation between the EPC-CFU count and *SMN2* copy numbers was detected ($r^2 = 0.1696$, P=0.1435) (Figure 5F).

This result indicates a decreased potential for endothelial repair in SMA patients. The lack of correlation between SMN2 copy number and the number of EPC-CFU indicates that a decreased potential for endothelial repair might be a general phenomenon in a range of SMA patients. Taken together, SMA patients show defective microvascular networks, increased vascular injury and a reduced capacity for vascular repair, consistent with a generalised microvasculopathy.

Antisense treatment ameliorates vascular repair defects in endothelial progenitor cells isolated from SMA patients

As intrathecal delivery of the AON nusinersen is used for treatment in SMA, and our observation that systemic AON treatment was able to rescue retinal vascularity in SMA mice, we next set out to investigate if AON treatment was able to rescue SMA-associated vasculopathy *in-vitro*. We tested the effect of SMN enhancing AON treatment on the defective EPC function in SMA patients. We treated patient-derived EPCs with a 25-mer AON (same sequence as used in mouse retina studies above) targeting ISS-N1 in *SMN2* intron 7 (21). To avoid the potential confounding effect of transfection reagents, this AON was synthesized in vivo-morpholino chemistry (VMO25), as described previously (21). EPCs isolated from Type 1 SMA patients (SMA-I, n=5) were treated with VMO25 (SMA-

I+VMO25) at 1μM for 7 days in the EPC-CFU assay. VMO25 significantly increased the number of EPC-CFU approximately 2-fold (15 CFUs/well, range 12-17) when compared to scrambled vivo-morpholino-treated (SMA-I+Scr-VMO, 7 CFUs/well, range 4-15, $P<0.05$) and untreated patients' EPCs (9 CFUs/well, range 2-13, $P<0.05$) (Figure 5G). This suggests that to ameliorate systemic SMA vasculopathy, the systemic administration of AON is required.

Endothelial cell-autonomous defects in angiogenesis drive the vascular phenotype

The findings detailed above all point to defects in angiogenesis, increased degeneration, and poor regeneration responses in the microvascular system of SMA patients. We therefore wanted to establish whether this represents a cell-autonomous endothelial phenotype, secondary to low levels of SMN protein. To understand the nature of the association between SMN and defective vascularity, we first performed a series of *in vitro* studies on angiogenesis in cultured human umbilical vein endothelial cells (HUVECs). As these are human cells carrying both *SMN1* and *SMN2* genes, we used an 18-mer exon 7-skipping AON to reduce SMN protein levels (Figure 6A) (52). This exon-skipping AON binding to both *SMN1* and *SMN2* pre-mRNA was synthesized in vivo-morpholino chemistry (E7-VMO), as above. After 48 hours incubation, 1 μm E7-VMO induced approximately 70% exon-skipping in *SMN1* and *SMN2* in HUVECs compared to scrambled control (Scr-VMO), as measured by quantitative reverse transcription PCR (Figure 6B).

We then used this E7-VMO to deplete SMN in HUVECs and investigate microvascular network formation and cell migration. HUVECs were initially incubated in Matrigel for 24 h at 37°C, followed by the treatment of E7-VMO or Scr-VMO at 1 μM for 48 hours. HUVECs treated with E7-VMO showed significantly (~50%) reduced HUVEC capillary network

formation as compared to untreated (Blank control) and Scr-VMO treated HUVECs (Figure 6C).

The ability of endothelial cells to migrate, which is key to angiogenesis, was measured by the scratch migration assay (53). HUVEC migration was significantly reduced after E7-VMO treatment (11.5±0.65, n=4) compared to Scr-VMO control (23.5±1.32, n=4; P=0.002) and blank control (28.6±2.30, n=5; P<0.0001) (Figure 6D). These data suggest that a depletion of SMN protein in cultured endothelial cells results in defective tube formation and migration, both essential components of angiogenesis. As this effect is directly linked to SMN deficiency, we concluded this represents a cell-autonomous defect.

We further confirmed the occurrence of the endothelial cell-autonomous defects in cells derived from SMA mice. Endothelial cells were isolated from the aorta of SMA mice and control littermates at P4-P6, and placed into culture. Cells were grown in Matrigel for 16 h to test their ability to form tubes. SMA endothelial cells showed significantly reduced tube formation (Figure 6E). The percentage of the total area covered by vessels was reduced by approximately 50% (Control: 24.57±1.06, SMA: 12.49±1.22, P<0.01), there was less branching, as the number of junctions were reduced by approximately 60% (Control: 159.7±26.49, SMA: 66.7±11.4, P<0.05), while lacunarity (the mesh size of the spaces in the vessel network) was approximately 3 times greater in control (1.09±0.22) compared with SMA (0.38±0.03, P<0.05) cultures. Although not statistically significant, SMA cultures also tended to have fewer end points (tubes terminating in a growing tip: Control: 152±24.01, SMA: 91.3±11.98, P=0.08, Figure 6F). Taken together, these data confirm an endothelial cell-autonomous defect in response to reduced SMN protein levels resulting in reduced angiogenesis.

Discussion

In this study, we have identified and characterised microvascular defects in SMA, investigated by imaging, histological, molecular and cellular studies in SMA patients, transgenic SMA mice and cellular models with SMN deficiency. We reveal a widespread microvascular pathology which is amendable to systemically-delivered SMN-restoring therapy, and describe gross and cellular biomarkers of vascular pathology.

The eye and neural retina are a window on the brain, and an area of growing interest in neurodegenerative diseases (29,54, 55), including motor neuron disease (56). However, retinal microvasculature has not previously been examined in SMA, even though there are changes in CNS neuronal and vascular parameters in SMA (22, 28). Here, by analysing ultra-widefield ophthalmoscopy images, we were able to detect a retinal vascular phenotype in children with SMA. Although the long-term biological implications of this finding in children are unknown, a lower FD in the retinal implicates subclinical microvascular changes in the systemic vasculature (57, 31). While FD is a promising measure for capturing the state of the vascular geometry, there are limitations to its computation using the method of automatic vessel detection or segmentation. We therefore applied two vessel segmentation methods to evaluate the stability of observations of statistically significant changes in FD. The key difference between the two techniques is the amount of vasculature that is detected. The Pellegrini technique (previous version of VAMPIRE-UWF) performs well on segmenting the larger and more prominent vessels whereas the IterNet technique (current version of VAMPIRE-UWF) segments both the prominent and the smaller vessels. Therefore, the IterNet technique includes more of the vasculature in FD computation than the Pellegrini technique. We believe the influence of including a more complete detection of the vasculature in FD computation is the contributing factor to a significant difference in the posterior ROI that was not observed in the Pellegrini technique as this region contains

numerous small vessels. In addition, recent work reported a non-uniform FD (obtained from Pellegrini segmentation) in the four retinal quadrants and a decrease in FD with increasing distance from the fovea in UWF retinal images from healthy people (58), therefore between ROI difference is not unexpected. However, it is not clear how this may relate to specific clinical vulnerability of different retinal regions which may have different metabolic demand for perfusion.

In SMA mice, widespread tissue hypoxia and multi-organ cellular hypoxic response have been previously demonstrated in both CNS and periphery (28). This was accompanied by increased glucose uptake in many affected organs, including spinal cord and eyes, as part of the hypoxia response (28). Hypoxia response is usually started by hypoxia induced factor (HIF) -1 and HIF-2 (59). However, no upregulation of HIF-1α or HIF-2 protein was detected in either of the hypoxic organs in SMA mice at the time point of the analysis (Supplemental Figure 3), suggesting tissue hypoxia is a rather complex dynamic cellular process under SMN deficiency. We have nevertheless showed that the widespread tissue hypoxia is associated with increased neuronal vulnerability to hypoxia in SMA mice (28). It is hypothesized that a disrupted neurovascular unit, consisting of local neurons, astrocytes and vascular endothelial cells, could exist in SMA (60). Indeed, the disruption of neuron-astrocyte-endothelial communication has recently been reported in both Alzheimer's disease (31, 61) and ALS (62). Early capillary regression results in insufficient local capillary blood flow and hypoxia (22), and we suggest that the reduced vascular tissue perfusion might in turn accelerate neuronal loss, leading to a vicious cycle involved in SMA disease progression. Further, defects in astrocyte to neuron communication in SMA (63), may also affect astrocyte to retinal ganglion cell interactions in the retina. Finally, microgliosis was initially reported in SMA mouse ventral horn (64), the effect of SMN depletion in microglia has been highlighted (65), and microglia are identified by GSL I/ IB4 stain following ischaemia (66). These

observations suggest an intrinsic and an extrinsic origin for microgliosis in SMA, which is particularly associated with synapse loss. This fits with our observation of an increase in microglia observed in the deeper layers of the retina, where neurons are lost. These observations suggest that the microgliosis seen in SMA mouse retinas may be indicative of a more broadly relevant phenotype in SMA.

Although we could not perform retinal imaging in Type 1 SMA infants due to the positioning compliance needed, we anticipate that the retinal vasculature abnormalities are likely to be present also in this severe form of SMA. The alterations in retinal vasculature in the milder children with SMA Types 2 and 3 are in keeping with the nature of the reported anomalies in retinal vasculature in SMA mouse models, though mice develop their vasculature postnatally in contrast to human infants who have retinal vasculature reaching the retinal periphery by term (67).

The identification of the retinal vascular phenotype is timely as detailed ocular surveillance has recently been put in place for SMA patients receiving risdiplam, due to the observation of retinal toxicity in preclinical toxicology studies (68). Reassuringly, neither the photoreceptor degeneration nor microcystoid macular degeneration, previously detected in treated monkeys, were seen in risdiplam treated patients (69). The study did include fundus photography, but the vascularity of the retina was not analysed. The less complex and less dense vasculature we quantified in SMA patients may not be obvious by direct inspection of an individual fundus image without FD analysis. Further analysis of the vasculature of these retinal images may provide more valuable information in this patient group. Future work to assess the extent of the microvascular structure defect in other anatomical localisation, for example the nailbed capillaries which can be assessed non-invasively using a capillaroscopy system (70, 71), would also be of interest.

Our studies demonstrate that there is an imbalance in endothelial injury and repair in SMA, as indicated by increased numbers of CECs, and decreased numbers of EPCs in SMA patient blood (Figure 5). CECs have been used as a marker to track endothelial injury in a wide range of acquired vascular disorders (46, 72), but never in SMA. We demonstrate that in SMA patients there was a correlation between the *SMN2* copy number and the increased CEC number, indicating the potential of CEC concentration in blood as a cellular biomarker of endothelial injury in SMA (Figure 5). Bone marrow-derived EPCs play an important role in endothelial maintenance and vascular healing (50), and act as a cellular biomarker of endothelial repair in various vascular diseases (43, 51, 73). The decreased EPC-CFU numbers in SMA patients (Figure 5D, E) and the sensitive response of cultured EPCs isolated from SMA Type 1 patients to AON treatment *in vitro* (Figure 5G), further support EPC as a potential cellular marker indicative of endothelial repair in SMA.

Finally, we revealed defective angiogenesis in cultured SMN-depleted endothelial cells, indicative of a cell-autonomous, SMN dependent pathology. While cell-autonomous defects secondary to SMN deficiency have been reported in key components of the motor system, including motor neurons (74), skeletal muscle satellite cells (75) and Schwann cells (76), there are no data on the vascular system. We demonstrate that cultured human endothelial cells with induced SMN deficiency display defects in vascular tube formation and endothelial cell migration (Figure 6A-D), but not endothelial cell apoptosis (Supplemental Figure 4). The cell autonomous defect was further confirmed in endothelial cells isolated from the aorta of SMA mice, which also showed reduced vascular tube formation (Figure 6E, F), a surrogate for angiogenesis. These data confirm the angiogenic phenotype described in the mouse retinal data, where the amount of outgrowth and number of growing tips of the vascular plexus were both depleted (Figure 2). In addition, the absence of vessel loss, failure of vessels

to mature and disorganised vessel growth, all point toward a primary failure in the ability of endothelial cells to grow and develop.

Our study indicates that microvasculopathy is a widespread phenomenon in patients and mice affected by SMA. This microvasculopathy is driven by an endothelial cell-autonomous defect in angiogenesis. This likely accelerates disease progression by further compromising organs that are already affected by SMN deficiency. Our findings emphasize the importance of therapeutic intervention to address the peripheral manifestation of SMA in addition to the central nervous system. While some therapies target both the periphery and CNS (10, 68), their effect on the vascular phenotype is still unknown. Onasemnogene abeparvovec has shown efficacy in restoring motor function and survival in Type 1 SMA patients, especially when administered close to disease onset (10). However, its limitation in rescuing the vascular-related clinical features (digit necrosis and diffuse macular rash) was highlighted in a recent report of a child with SMA Type 0 who was treated with both nusinersen and onasemnogene abeparvovec. These peripheral manifestations remained unchanged, despite the modest motor improvement (77). Whilst AAV9 serotype is efficient in crossing the BBB, it induces minimal transduction of endothelial cells, while maintaining the capacity to transduce neurons after the endothelial transcytosis (78). Of relevance, thrombotic microangiopathy (TMA), characterized by arteriole and capillary endothelial pathology and microvascular thrombosis, is a severe adverse effect recently reported in several SMA infants treated with onasemnogene abeparvovec (79). While the exact mechanism of this adverse reaction is still unknown, suggested etiologies include direct AAV toxic effect (80), or immune-mediated reactions to AAV vector (81). Our finding provides a further explanation and indicates that the underlying endothelial dysfunction in SMA may predispose some patients to TMA following systemic AAV gene therapy. To reduce the incidence of TMA, it

would be important to evaluate the baseline vascular status of patients before commencing AAV-mediated treatment, as this might help to identify potentially susceptible individuals.

Taken together, our data identify microvasculopathy as a fundamental feature of SMA, which is driven by reversible autonomous endothelial cell defect. Future studies on endothelial cell-specific SMN restoration in SMA mice will be needed to better understand the role of endothelial cells in disease pathogenesis and progression, and to what extent that microvasculopathy may contribute to the multi-organ involvement in SMA. In light of all these findings, our study suggests that therapeutic strategies for SMA should also include the correction of the SMN deficiency in the periphery, including the vascular system.

Materials and Methods

Patients and controls

All studies were performed in children with SMA with different levels of clinical severity attending the Great Ormond Street Hospital NHS Foundation Trust, London during Oct 2015 and Feb 2018. Parental consent was obtained for all children involved in the study, which was approved by the national Ethics Committees (See Study Approval). Inclusion criteria for children with SMA were as follows: age <18 years, a diagnosis of SMA confirmed by genetic diagnosis indicating a genomic deletion in the *SMN1* gene. Control samples were obtained from healthy sex- and age-matched children.

SMA mice and procedures

SMA transgenic mice, FVB.Cg-Tg(*SMN2*)$_2$Hung *Smn1*^{tm1Hung}/J, also called the Taiwanese model (35), were initially purchased from Jackson Laboratory (TJL005058; Jackson Laboratory, Bar Harbor, ME). Mice were bred and experimental procedures were carried out in the Biological Service Unit, University College London, in accordance with the Animals (Scientific Procedures) Act 1986.

Newborn SMA mice were subcutaneously injected a single dose of PMO25 at 40 μg/g. Untreated SMA control mice were injected with similar volume of saline as previously described (21).

Antisense oligonucleotides

The therapeutic AON PMO25 and the *SMN1/2* exon 7 skipping vivo-morpholino (E7-VMO) were purchased from Gene Tools. The antisense sequences were listed in Supplemental Table 1.

Human retina imaging and data analysis

An ultra-widefield (UWF) scanning laser ophthalmoscope (California CA Optos plc., Dunfermline, Scotland, UK) was used to take non-dilated fundus images of the retinae of 11 SMA patients Type 2 (n=6) and Type 3 (n=5), median age 11yrs (range 6-16yrs), and from 23 healthy controls, median age 9yrs (range 3.5-17yrs). The plot of ages was presented in Supplemental Figure 5. These images were centred on the fovea with on-axis symmetry of 15 μm (TIFF format; 4000 × 4000 pixels). Measurements of the vasculature were obtained using specially designed software for analysing UWF images (Vasculature Assessment and Measurement Platform for Images of the Retina (version VAMPIRE-UWF), Universities of Edinburgh and Dundee, UK).

Fractal dimension (FD) is a unitless measure between 1-2. It describes how a repeating pattern (such as the retinal vasculature) fills the space in which it is contained. FD is influenced by: (1) the space or region of interest (ROI) in which it is measured (e.g., FD of a branching pattern may decrease if the space in which it is contained increases – i.e., filling the larger space less); (2) accuracy of the vessel segmentation and (3) image quality (that directly affects (2)). We therefore standardised the ROI (provided by the VAMPIRE-UWF software) so that FD was computed for the same area within each image (denoted *Standardised ROI).(Figure 1 shows this region highlighted on the UWF image in grey.)* We only included images clear from eyelashes and eyelids, that can interfere with analysis, resulting in 21 images from SMA patient eyes and 46 control eyes. Next, the retinal vessels were automatically segmented from the background using two different methods (33, 34). The Pellegrini *et al*. 2014 method segments prominent vessels and the IterNet 2020 method segments prominent and the smaller branching vessels. The segmented images were then skeletonised (i.e., the centreline of the vessel network was represented as 1-pixel wide curved lines). The difference in vessel skeletons from the two different segmentation methods can be seen in Figure 1. The skeletons were inspected and any minor erroneous segmentations corrected manually. The *Standardised* ROI, (VAMPIRE-

UWF), has an area of 319 mm^2 and includes the posterior pole, midperiphery and small portion of the far periphery. The *Standardized* ROI was subdivided into a *Posterior* ROI (an annulus centred on the optic disc that extends three optic disc diameters away from the optic disc boundary also known as zone C (82) and a *Midperiphery* ROI (area between *Standardised* and *Posterior* ROI) to investigate regional changes in FD. FD was computed from the three regions using methods reported previously (83).

Mouse retinas dissection and immunohistochemical staining. See Supplemental Methods.

Quantification of mouse retinal vascularity

AngioTool software was used for quantification of the retinal vasculature (https://ccrod.cancer.gov/confluence/display/ROB2/Home). For vessel outgrowth a single figure was obtained for each retina. For Endpoint number and lacunarity, a systematic and random method was used to capture ROIs for assessment, and thus each data point represents a single field.

Quantification of mouse retinal thickness and retinal cells

Stained slides of mouse retinas were imaged using a standard upright Nikon Eclipse E400 microscope. Images were captured using a QICAM Fast 1394 camera and Volocity imaging software (PerkinElmer). Retinal thickness was measured directly from calibrated images. Retinal cell density was calculated using a systematic, random methodology, based on a method reported previously (84). Additional details are presented in the Supplemental Methods

Immunomagnetic bead extraction of circulating endothelial cells from peripheral blood

CECs were extracted from whole blood by CD146-coated immunomagnetic beads (5050-P, BioCytex, Marseille, France) using an international consensus protocol (45). The extracted

CECs were counted using a Nageotte chamber under a fluorescence microscope and were defined as Ulex europaeus lectin (L9006, Sigma-Aldrich, Doset, UK) bright cells that were > 10 μm in size, with five or more magnetic beads attached.

Endothelial progenitor cell colony-forming units

Peripheral blood mononuclear cells (PBMC) were isolated by density centrifugation (Lymphoprep TM, Axis Shield, Dundee, UK). After purification with three washing steps, 2 × 10^6 PBMCs were plated on fibronectin-coated 24-well plates. Cells were cultured and maintained in endothelial growth medium (EGM-2) supplemented with growth factors according to the manufacturer's recommendations (PromoCell, Heidelberg, Germany), plus 20 % foetal calf serum (FCS) and 40 ng/ml of vascular endothelial growth factor (VEGF). After four days of culture, non-adherent cells were removed by washing with PBS.

To study the effects of AONs, 1 μM VMO25 or Scr-VMO was added to the media at day 4. Culture medium was changed to maintain the cells in culture until day 7. The numbers of EPC-CFU, characterized by a cluster of cells surrounded by elongated spindled-shaped cells, were counted manually in a minimum of two wells in 24-well plates by two independent observers who were unaware of the experiment design. Results were presented as average number of EPC-CFUs per well.

HUVEC cultures and induced *SMN1* and *SMN2* Exon 7-skipping by vivo-morpholino. See Supplemental Methods.

HUVEC tube formation and cell migration assay. See Supplemental Methods.

SMA mouse endothelial cell cultures and tube formation assay. See Supplemental Methods.

PCR, real-time PCR and western blotting. See Supplemental Methods.

Statistics

For data collected from SMA patients and controls, numeric results were summarized as median and range. The D'Agostino and Pearson omnibus normality test was used to examine overall differences in experimental laboratory markers between the study groups, followed by the two-tailed Mann-Whitney *U* test. Associations between CECs and EPCs with *SMN2* copy numbers were assessed using Spearman rank correlation coefficient.

Statistical analysis of human retinal parameters was conducted using generalised estimation equations (GEE's; R version 3.6.0; geepack (85)) (86), that accounts for the correlation between both eyes of an individual. As GEE's are sensitive to outliers, extreme values were imputed to the mean of the group (87).

All *in vitro* experiments were performed in triplicate unless otherwise stated, and values are presented as mean ± standard error of the mean (SEM) unless otherwise specified. Statistical differences between two groups for *in vitro* experiments and *in vivo* studies in mice were determined by unpaired two-tailed Student's T-test; statistical analysis in more than two groups were performed by one-way analysis of variance (ANOVA) followed by post-hoc Tukey test. A *P* value less than 0.05 was considered significant. All analysis was performed using GraphPad Prism software.

Study approval

The study was approved by the national ethics committees, including the West London & GTAC Research Ethics Committee (REC reference 06/Q0406/33), NRES Committee London - Camberwell St Giles (REC reference 13/LO/1894) and NRES Committee London – Bromley (REC reference 13/LO/1748). Blood samples were supplied by the MRC Centre for Neuromuscular Diseases Biobank London (http://www.cnmd.ac.uk). All participants provided written, fully informed consent prior to inclusion in the study. All participants were

anonymous in this study. Experiments on animals were performed under Home Office project licences PP2611161 and P92BB9F93. All treatment procedures conducted in mice were carried out in the Biological Services Unit, University College London Great Ormond Street Institute of Child Health, in accordance with the Animals (Scientific Procedures) Act 1986.

Author contributions

HZ, YH, PB, THG, DT, SHP and FM conceived and designed the research studies. HZ, YH, AT, DT, EP, TM, EH, MS, FC, GH, HS, TN, JEM, JM, QZ and AH conducted the experiments and analyzed the data. MS and GB provided clinical samples and data. HZ, SHP, THG, KH, PB, DT and FM wrote the manuscript. HZ, YH, MS, AT, and EP agreed to share the first-authorship due to their important contribution and heavy involvement in conducting the experiments, data analysis and presenting the results.

Acknowledgments

We would like to thank Professor Peter Carmeliet at University of Leuven and Prof Martin Collinson at University of Aberdeen for help with mouse retina dissection and staining, and Professor Jennifer E. Morgan at University College London for overseeing experiments in mice. This study was supported in part by research funding from the Great Ormond Street Hospital Charity to FM and PB (Reference V0216), Wellcome Trust grant to HZ (Reference 204841/Z/16/Z), EU H2020-MSCA-ITN-2020 grant to FM, HZ and THG (SMABEYOND, 956185), UK SMA Trust to FM and MS, SMA Europe grants to FM, HZ, THG and SHP, and Anatomical Society PhD Studentship to SHP. Financial support from the NIHR Biomedical Research Centre at Great Ormond Street Hospital and University College London to FM and HZ is acknowledged. The supports of the MRC Neuromuscular Centre at UCL and of the Muscular Dystrophy UK to the Dubowitz Neuromuscular Centre are also acknowledged.

References

1. Lefebvre S, Bürglen L, Reboullet S, Clermont O, Burlet P, Viollet L, et al. Identification and characterization of a spinal muscular atrophy-determining gene. *Cell.* 1995;80(1):155-65.
2. Dubowitz V. Ramblings in the history of spinal muscular atrophy. *Neuromuscul Disord.* 2009;19(1):69-73.
3. Feldkötter M, Schwarzer V, Wirth R, Wienker TF, and Wirth B. Quantitative analyses of SMN1 and SMN2 based on real-time lightCycler PCR: fast and highly reliable carrier testing and prediction of severity of spinal muscular atrophy. *Am J Hum Genet.* 2002;70(2):358-68.
4. Mercuri E, Pera MC, Scoto M, Finkel R, and Muntoni F. Spinal muscular atrophy - insights and challenges in the treatment era. *Nat Rev Neurol.* 2020;16(12):706-15.
5. Finkel RS, Chiriboga CA, Vajsar J, Day JW, Montes J, De Vivo DC, et al. Treatment of infantile-onset spinal muscular atrophy with nusinersen: a phase 2, open-label, dose-escalation study. *Lancet.* 2016;388(10063):3017-26.
6. Mercuri E, Darras BT, Chiriboga CA, Day JW, Campbell C, Connolly AM, et al. Nusinersen versus Sham Control in Later-Onset Spinal Muscular Atrophy. *N Engl J Med.* 2018;378(7):625-35.
7. Hua Y, Vickers TA, Okunola HL, Bennett CF, and Krainer AR. Antisense masking of an hnRNP A1/A2 intronic splicing silencer corrects SMN2 splicing in transgenic mice. *Am J Hum Genet.* 2008;82(4):834-48.
8. Singh NK, Singh NN, Androphy EJ, and Singh RN. Splicing of a critical exon of human Survival Motor Neuron is regulated by a unique silencer element located in the last intron. *Mol Cell Biol.* 2006;26(4):1333-46.
9. Foust KD, Wang X, McGovern VL, Braun L, Bevan AK, Haidet AM, et al. Rescue of the spinal muscular atrophy phenotype in a mouse model by early postnatal delivery of SMN. *Nat Biotechnol.* 2010;28(3):271-4.
10. Mendell JR, Al-Zaidy S, Shell R, Arnold WD, Rodino-Klapac LR, Prior TW, et al. Single-Dose Gene-Replacement Therapy for Spinal Muscular Atrophy. *N Engl J Med.* 2017;377(18):1713-22.
11. Valori CF, Ning K, Wyles M, Mead RJ, Grierson AJ, Shaw PJ, et al. Systemic delivery of scAAV9 expressing SMN prolongs survival in a model of spinal muscular atrophy. *Sci Transl Med.* 2010;2(35):35ra42.
12. Naryshkin NA, Weetall M, Dakka A, Narasimhan J, Zhao X, Feng Z, et al. Motor neuron disease. SMN2 splicing modifiers improve motor function and longevity in mice with spinal muscular atrophy. *Science.* 2014;345(6197):688-93.
13. Baranello G, Darras BT, Day JW, Deconinck N, Klein A, Masson R, et al. Risdiplam in Type 1 Spinal Muscular Atrophy. *N Engl J Med.* 2021;384(10):915-23.
14. Groen EJN, Talbot K, and Gillingwater TH. Advances in therapy for spinal muscular atrophy: promises and challenges. *Nat Rev Neurol.* 2018;14(4):214-24.
15. Hamilton G, and Gillingwater TH. Spinal muscular atrophy: going beyond the motor neuron. *Trends Mol Med.* 2013;19(1):40-50.
16. Shababi M, Lorson CL, and Rudnik-Schöneborn SS. Spinal muscular atrophy: a motor neuron disorder or a multi-organ disease? *J Anat.* 2014;224(1):15-28.
17. Yeo CJJ, and Darras BT. Overturning the Paradigm of Spinal Muscular Atrophy as Just a Motor Neuron Disease. *Pediatr Neurol.* 2020;109:12-9.
18. Araujo A, Araujo M, and Swoboda KJ. Vascular perfusion abnormalities in infants with spinal muscular atrophy. *J Pediatr.* 2009;155(2):292-4.
19. Rudnik-Schöneborn S, Vogelgesang S, Armbrust S, Graul-Neumann L, Fusch C, and Zerres K. Digital necroses and vascular thrombosis in severe spinal muscular atrophy. *Muscle Nerve.* 2010;42(1):144-7.
20. Weissman AS, Kennedy KR, Powell MR, and Davis LS. Skin necrosis in spinal muscular atrophy: Case report and review of the literature. *Pediatr Dermatol.* 2021;38(3):632-636

21. Zhou H, Janghra N, Mitrpant C, Dickinson RL, Anthony K, Price L, et al. A novel morpholino oligomer targeting ISS-N1 improves rescue of severe spinal muscular atrophy transgenic mice. *Hum Gene Ther.* 2013;24(3):331-42.
22. Somers E, Lees RD, Hoban K, Sleigh JN, Zhou H, Muntoni F, et al. Vascular Defects and Spinal Cord Hypoxia in Spinal Muscular Atrophy. *Ann Neurol.* 2016;79(2):217-30.
23. Sintusek P, Catapano F, Angkathunkayul N, Marrosu E, Parson SH, Morgan JE, et al. Histopathological defects in intestine in severe spinal muscular atrophy mice are improved by systemic antisense oligonucleotide treatment. *PLoS One*. 2016;11:e0155032.
24. Somers E, Stencel Z, Wishart TM, Gillingwater TH, and Parson SH. Density, calibre and ramification of muscle capillaries are altered in a mouse model of severe spinal muscular atrophy. *Neuromuscul Disord.* 2012;22(5):435-42.
25. Maxwell GK, Szunyogova E, Shorrock HK, Gillingwater TH, and Parson SH. Developmental and degenerative cardiac defects in the Taiwanese mouse model of severe spinal muscular atrophy. *J Anat.* 2018;232(6):965-78.
26. Bevan AK, Hutchinson KR, Foust KD, Braun L, McGovern VL, Schmelzer L, et al. Early heart failure in the SMNDelta7 model of spinal muscular atrophy and correction by postnatal scAAV9-SMN delivery. *Hum Mol Genet.* 2010;19(20):3895-905.
27. Shababi M, Habibi J, Yang HT, Vale SM, Sewell WA, and Lorson CL. Cardiac defects contribute to the pathology of spinal muscular atrophy models. *Hum Mol Genet.* 2010;19(20):4059-71.
28. Hernandez-Gerez E, Dall'Angelo S, Collinson JM, Fleming IN, and Parson SH. Widespread tissue hypoxia dysregulates cell and metabolic pathways in SMA. *Ann Clin Transl Neurol.* 2020;7(9):1580-93.
29. Kobayashi DT, Shi J, Stephen L, Ballard KL, Dewey R, Mapes J, et al. SMA-MAP: a plasma protein panel for spinal muscular atrophy. *PLoS One.* 2013;8(4):e60113.
30. Kashani AH, Asanad S, Chan JW, Singer MB, Zhang J, Sharifi M, et al. Past, present and future role of retinal imaging in neurodegenerative disease. *Prog Retin Eye Res.* 2021;83:100938.
31. Lemmens S, Devulder A, Van Keer K, Bierkens J, De Boever P, and Stalmans I. Systematic Review on Fractal Dimension of the Retinal Vasculature in Neurodegeneration and Stroke: Assessment of a Potential Biomarker. *Front Neurosci.* 2020;14:16.
32. Mainster MA. The fractal properties of retinal vessels: embryological and clinical implications. *Eye (Lond).* 1990;4 (Pt 1):235-41.
33. Li L, Verma M, Nakashima Y, Nagahara H, and Kawasaki R. IterNet: Retinal Image Segmentation Utilizing Structural Redundancy in Vessel Networks. *IEEE Xplore*. 2020.
34. Pellegrini E, Robertson G, Trucco E, MacGillivray TJ, Lupascu C, van Hemert J, et al. Blood vessel segmentation and width estimation in ultra-wide field scanning laser ophthalmoscopy. *Biomed Opt Express.* 2014;5(12):4329-37.
35. Hsieh-Li HM, Chang JG, Jong YJ, Wu MH, Wang NM, Tsai CH, et al. A mouse model for spinal muscular atrophy. *Nat Genet.* 2000;24(1):66-70.
36. Zudaire E, Gambardella L, Kurcz C, and Vermeren S. A computational tool for quantitative analysis of vascular networks. *PLoS One.* 2011;6(11):e27385.
37. Streit WJ, Kreutzberg GW. Lectin binding by resting and reactive microglia. *Neurocytol.* 1987 Apr;16(2):249-60.
38. Zhou H, Meng J, Marrosu E, Janghra N, Morgan J, and Muntoni F. Repeated low doses of morpholino antisense oligomer: an intermediate mouse model of spinal muscular atrophy to explore the window of therapeutic response. *Hum Mol Genet.* 2015;24(22):6265-77.
39. Alves CH, Fernandes R, Santiago AR, and Ambrósio AF. Microglia Contribution to the Regulation of the Retinal and Choroidal Vasculature in Age-Related Macular Degeneration. *Cells.* 2020;9(5):1217.
40. Ito D, Imai Y, Ohsawa K, Nakajima K, Fukuuchi Y, and Kohsaka S. Microglia-specific localisation of a novel calcium binding protein, Iba1. *Brain Res Mol Brain Res*. 1998;57(1):1-9.

41. Clarke LA, Hong Y, Eleftheriou D, Shah V, Arrigoni F, Klein NJ, et al. Endothelial injury and repair in systemic vasculitis of the young. *Arthritis Rheum.* 2010;62(6):1770-80.
42. Evans CE, Iruela-Arispe ML, and Zhao YY. Mechanisms of Endothelial Regeneration and Vascular Repair and Their Application to Regenerative Medicine. *Am J Pathol.* 2021;191(1):52-65.
43. Hong Y, Eleftheriou D, Klein NJ, and Brogan PA. Impaired function of endothelial progenitor cells in children with primary systemic vasculitis. *Arthritis Res Ther.* 2015;17:292.
44. Brogan P, Eleftheriou D, and Dillon M. Small vessel vasculitis. *Pediatr Nephrol.* 2010;25(6):1025-35.
45. Clarke LA, Shah V, Arrigoni F, Eleftheriou D, Hong Y, Halcox J, et al. Quantitative detection of circulating endothelial cells in vasculitis: comparison of flow cytometry and immunomagnetic bead extraction. *J Thromb Haemost.* 2008;6(6):1025-32.
46. Erdbruegger U, Haubitz M, and Woywodt A. Circulating endothelial cells: a novel marker of endothelial damage. *Clin Chim Acta.* 2006;373(1-2):17-26.
47. Eleftheriou D, Ganesan V, Hong Y, Klein NJ, and Brogan PA. Endothelial injury in childhood stroke with cerebral arteriopathy: a cross-sectional study. *Neurology.* 2012;79(21):2089-96.
48. Erdbruegger U, Dhaygude A, Haubitz M, and Woywodt A. Circulating endothelial cells: markers and mediators of vascular damage. *Curr Stem Cell Res Ther.* 2010;5(4):294-302.
49. Papadopoulou C, Hong Y, Krol P, Al Obaidi M, Pilkington C, Wedderburn LR, et al. The Vasculopathy of Juvenile Dermatomyositis: Endothelial Injury, Hypercoagulability, and Increased Arterial Stiffness. *Arthritis Rheumatol.* 2021;73(7):1253-66.
50. Asahara T, Murohara T, Sullivan A, Silver M, van der Zee R, Li T, et al. Isolation of putative progenitor endothelial cells for angiogenesis. *Science.* 1997;275(5302):964-7.
51. Hill JM, Zalos G, Halcox JP, Schenke WH, Waclawiw MA, Quyyumi AA, et al. Circulating endothelial progenitor cells, vascular function, and cardiovascular risk. *N Engl J Med.* 2003;348(7):593-600.
52. Sahashi K, Ling KK, Hua Y, Wilkinson JE, Nomakuchi T, Rigo F, et al. Pathological impact of SMN2 mis-splicing in adult SMA mice. *EMBO Mol Med.* 2013;5(10):1586-601.
53. Guo S, Lok J, Liu Y, Hayakawa K, Leung W, Xing C, et al. Assays to examine endothelial cell migration, tube formation, and gene expression profiles. *Methods Mol Biol.* 2014;1135:393-402.
54. Snyder PJ, Alber J, Alt C, Bain LJ, Bouma BE, Bouwman FH, et al. Retinal imaging in Alzheimer's and neurodegenerative diseases. *Alzheimers Dement.* 2021;17(1):103-11.
55. Xia F, Ha Y, Shi S, Li Y, Li S, Luisi J, et al. Early alterations of neurovascular unit in the retina in mouse models of tauopathy. *Acta Neuropathol Commun.* 2021;9(1):51.
56. Rojas P, Ramírez AI, Fernández-Albarral JA, López-Cuenca I, Salobrar-García E, Cadena M, et al. Amyotrophic Lateral Sclerosis: A Neurodegenerative Motor Neuron Disease With Ocular Involvement. *Front Neurosci.* 2020;14:566858.
57. Grassi G and Mancia G. 'Keep an eye' on the heart: retinal microcirculation disarray in congestive heart failure. *Eur Heart J*. 2018;39 (1):57–59.
58. Fan WY, Fleming A, Robertson G, Uji A, van Hemert J, Singer M, et al. Fractal analysis of retinal vasculature in normal subjects on ultra-wide field fluorescein angiography. *Int J Ophthalmol*. 2020;13(7):1109-1114.
59. Ratcliffe PJ. HIF-1 and HIF-2: working alone or together in hypoxia? *J Clin Invest*. 2007;117(4):862-5.
60. Nobutoki T, and Ihara T. Early disruption of neurovascular units and microcirculatory dysfunction in the spinal cord in spinal muscular atrophy type I. *Med Hypotheses.* 2015;85(6):842-5.
61. Zlokovic BV. Neurovascular pathways to neurodegeneration in Alzheimer's disease and other disorders. *Nat Rev Neurosci.* 2011;12(12):723-38.

62. Miyazaki K, Ohta Y, Nagai M, Morimoto N, Kurata T, Takehisa Y, et al. Disruption of neurovascular unit prior to motor neuron degeneration in amyotrophic lateral sclerosis. *J Neurosci Res.* 2011;89(5):718-28.
63. Zhou C, Feng Z, and Ko CP. Defects in Motoneuron-Astrocyte Interactions in Spinal Muscular Atrophy. *J Neurosci.* 2016;36(8):2543-53.
64. Tarabal O, Caraballo-Miralles V, Cardona-Rossinyol A, Correa FJ, Olmos G, Lladó J, et al. Mechanisms involved in spinal cord central synapse loss in a mouse model of spinal muscular atrophy. *J Neuropathol Exp Neurol*. 2014;73(6):519-35.
65. Khayrullina G, Alipio-Gloria ZA, Deguise MO, Gagnon S, Chehade L, Stinson M, et al. Survival motor neuron protein deficiency alters microglia reactivity. *Glia*. 2022 Jul;70(7):1337-1358.
66. Boscia F, Esposito CL, Casamassa A, Franciscis V, Annunziato L, and Cerchia L. The isolectin IB4 binds RET receptor tyrosine kinase in microglia. *J Neurochem*. 2013;126(4):428-36.
67. Sun Y, and Smith LEH. Retinal Vasculature in Development and Diseases. *Annu Rev Vis Sci.* 2018;4:101-22.
68. Ratni H, Ebeling M, Baird J, Bendels S, Bylund J, Chen KS, et al. Discovery of Risdiplam, a Selective Survival of Motor Neuron-2 (SMN2) Gene Splicing Modifier for the Treatment of Spinal Muscular Atrophy (SMA). *J Med Chem.* 2018;61(15):6501-17.
69. Sergott RC, Amorelli GM, Baranello G, Barreau E, Beres S, Kane S, et al. Risdiplam treatment has not led to retinal toxicity in patients with spinal muscular atrophy. *Ann Clin Transl Neurol.* 2021;8(1):54-65.
70. Cutolo M, Sulli A, and Smith V. How to perform and interpret capillaroscopy. *Best Pract Res Clin Rheumatol.* 2013;27(2):237-48.
71. Dolezalova P, Young SP, Bacon PA, and Southwood TR. Nailfold capillary microscopy in healthy children and in childhood rheumatic diseases: a prospective single blind observational study. *Ann Rheum Dis.* 2003;62(5):444-9.
72. Blann AD, Woywodt A, Bertolini F, Bull TM, Buyon JP, Clancy RM, et al. Circulating endothelial cells. Biomarker of vascular disease. *Thromb Haemost.* 2005;93(2):228-35.
73. Werner N, Kosiol S, Schiegl T, Ahlers P, Walenta K, Link A, et al. Circulating endothelial progenitor cells and cardiovascular outcomes. *N Engl J Med.* 2005;353(10):999-1007.
74. Gallotta I, Mazzarella N, Donato A, Esposito A, Chaplin JC, Castro S, et al. Neuron-specific knock-down of SMN1 causes neuron degeneration and death through an apoptotic mechanism. *Hum Mol Genet.* 2016;25(12):2564-77.
75. Hayhurst M, Wagner AK, Cerletti M, Wagers AJ, and Rubin LL. A cell-autonomous defect in skeletal muscle satellite cells expressing low levels of survival of motor neuron protein. *Dev Biol.* 2012;368(2):323-34.
76. Hunter G, Aghamaleky Sarvestany A, Roche SL, Symes RC, and Gillingwater TH. SMN-dependent intrinsic defects in Schwann cells in mouse models of spinal muscular atrophy. *Hum Mol Genet.* 2014;23(9):2235-50.
77. Matesanz SE, Curry C, Gross B, Rubin AI, Linn R, Yum SW, et al. Clinical Course in a Patient With Spinal Muscular Atrophy Type 0 Treated With Nusinersen and Onasemnogene Abeparvovec. *J Child Neurol.* 2020;35(11):717-23.
78. Merkel SF, Andrews AM, Lutton EM, Mu D, Hudry E, Hyman BT, et al. Trafficking of adeno-associated virus vectors across a model of the blood-brain barrier; a comparative study of transcytosis and transduction using primary human brain endothelial cells. *J Neurochem.* 2017;140(2):216-30.
79. Chand DH, Zaidman C, Arya K, Millner R, Farrar MA, Mackie FE, et al. Thrombotic Microangiopathy Following Onasemnogene Abeparvovec for Spinal Muscular Atrophy: A Case Series. *J Pediatr.* 2021;231:265-8.
80. Yabe H, Hattori K, Inoue H, Matsumoto M, Hamanoue S, Hiroi A, et al. Fatal adenovirus infection indistinguishable from thrombotic microangiopathy after allogeneic CD34+ peripheral progenitor cell transplantation. *Tokai J Exp Clin Med.* 2005;30(1):71-5.

81. Friese J, Geitmann S, Holzwarth D, Müller N, Sassen R, Baur U, et al. Safety Monitoring of Gene Therapy for Spinal Muscular Atrophy with Onasemnogene Abeparvovec -A Single Centre Experience. *J Neuromuscul Dis.* 2021;8(2):209-16.
82. Frost S, Kanagasingam Y, Sohrabi H, Vignarajan J, Bourgeat P, Salvado O, et al. Retinal vascular biomarkers for early detection and monitoring of Alzheimer's disease. *Transl Psychiatry.* 2013;3(2):e233.
83. Stosić T, and Stosić BD. Multifractal analysis of human retinal vessels. *IEEE Trans Med Imaging.* 2006;25(8):1101-7.
84. Mayhew TM and Sharma AK. Sampling schemes for estimating nerve fibre size. II. Methods for unifascicular nerve trunks. *J Anat*. 1984;139(Pt 1):59-66.
85. Yan J. geepack: Yet Another Package for Generalized Estimating Equations. *R-News.* 2002;2/3:12-4.
86. Ying GS, Maguire MG, Glynn R and Rosner B. Tutorial on Biostatistics: Statistical Analysis for Correlated Binary Eye Data. *Ophthalmic Epidemiol*. 2018;25(1):1-12.
87. NISA KH, Netti. Robust Estimation of Generalized Estimating Equation when Data Contain Outliers. *INSIST.* 2017;2:1-5.

Figures and Legends

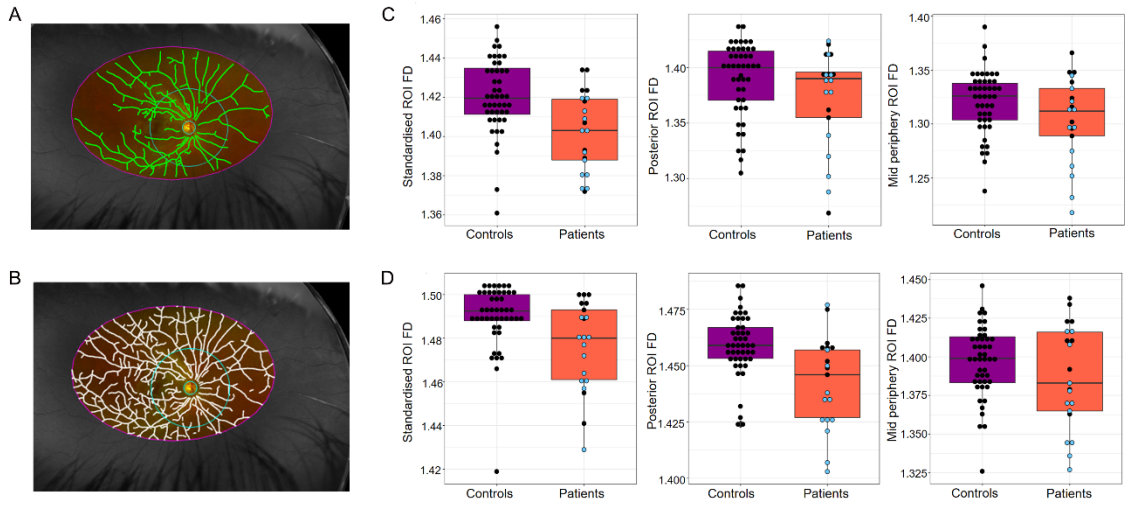

Figure 1 Retinal imaging and data analysis in SMA patients.

The vessel skeletons produced using two different automatic vasculature segmentation methods are shown: **(A)** Skeleton (in green) from methods of *Pellegrini et al* (34) segments only prominent vessels in the image; **(B)** Skeleton (in white) using *Iternet neural network* (33) segments discrete and prominent vessels. Ultra-wide field retinal images in grey scale are shown from the right eye of the same individual. Fractal dimensions (FD) were calculated by segmentation method of *Pellegrini et al* **(C)** and *Iternet neural network* **(D)** from three regions of interest (ROI) outlined by coloured lines: standardized ROI (magenta outline), Posterior ROI (cyan outline around the optic nerve head) and Midperiphery ROI (between cyan to magenta). For each segmentation method three box plots show the distribution of corresponding FD calculated from each ROI in SMA patients (orange box, n=21) compared to controls (magenta box, n=46). Type 2 SMA patients in blue dots (n=12), Type 3 in black dots (n=9).

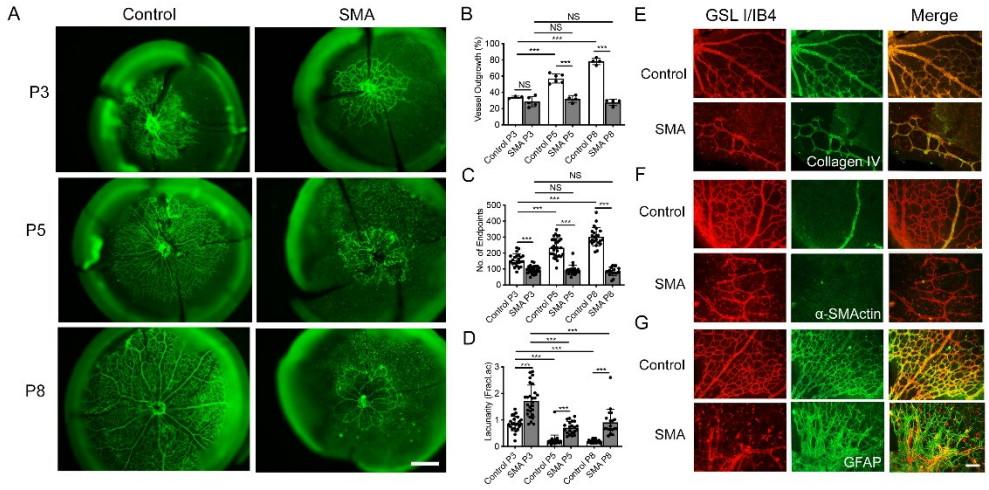

907

908 **Figure 2 Abnormal post-natal Development of retinal vasculature in a mouse**
909 **model of SMA**

910 (**A**) Retinas were collected from SMA mice and healthy littermate controls at P3, P5 and P8,
911 and stained with GSL I/IB4 lectin (green). Quantification of the retinal vasculature using
912 AngioTool on (**B**) vessels outgrowth, (**C**) number of microvessel endpoints and (**D**)
913 lacunarity in SMA retinas compared to controls at P3, P5 and P8. (**E**) Co-staining for vessels
914 with GSL I/IB4 (red) and basement lamina with collagen IV (green). (**F**) Co-staining for
915 vessels with GSL I/IB4 (red) and smooth muscle with α-smooth muscle actin (αSMActin,
916 green). (**G**) Co-staining for vessels with GSL I/IB4 (red) and astrocytes with Glial fibrillary
917 acidic protein (GFAP, green). All images were taken from retinas from mice at P8. Data
918 represent mean ±SEM with individual data points displayed, from ≥3 mice for each group.
919 Scale bar = 500 µm in **A** and 50 µm in **G**. One way ANOVA with Tukey post-hoc test was
920 used for data analyse. * P< 0.05, **P<0.01, *** P<0.001.

921

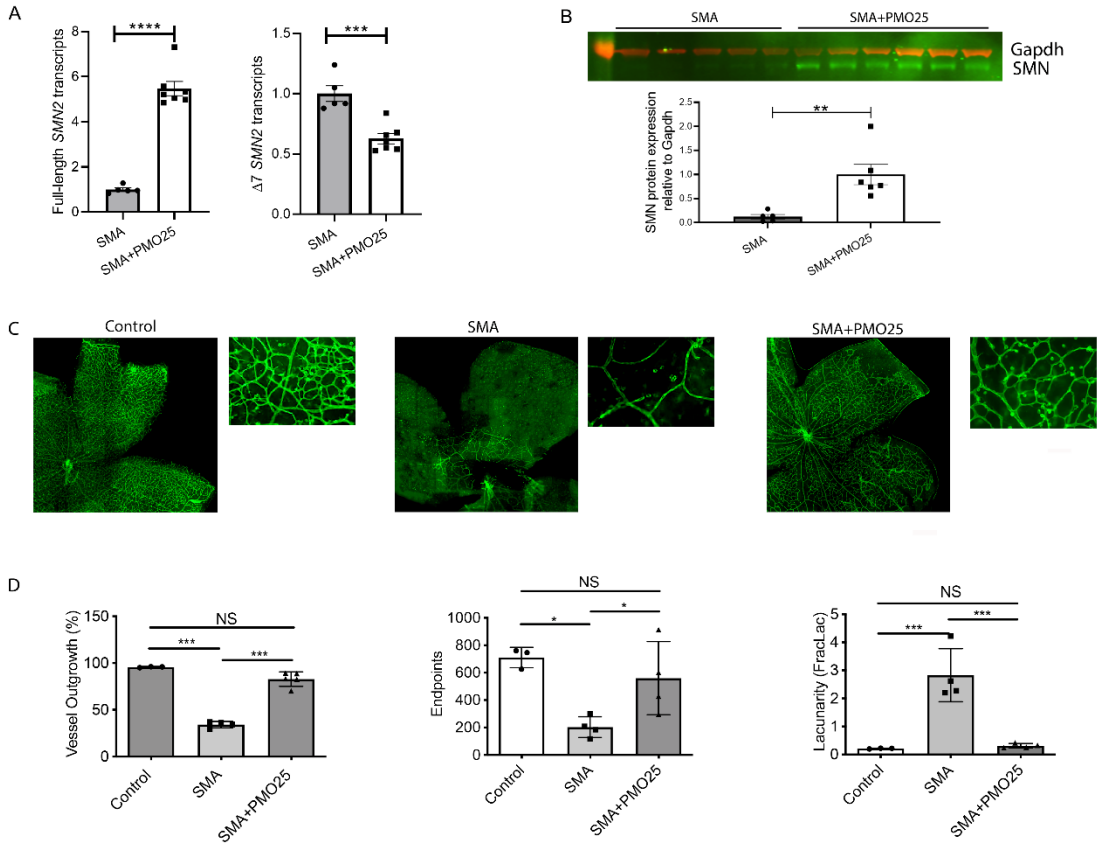

Figure 3 SMN restoration with antisense treatment restores retinal vasculature in SMA mice

(**A**) The full-length *SMN2* transcripts and truncated *SMN2* transcripts without exon 7 (Δ7 SMN2) were measured by quantitative real-time PCR in retinas collected from PMO25-treated SMA mice (SMA+PMO25, n=7), compared to saline-treated SMA mice (n=5). (**B**) A representative image of western blotting and semi-quantification of SMN protein expression in mouse retinas from SMA mice after PMO25 treatment (n=6), compared to saline treated SMA controls (n=5). Mouse Gapdh protein was used as a loading control. (**C**) Mouse retinas from saline-treated SMA, PMO25-treated SMA and healthy littermate controls were stained with GSL I/IB4 lectin (Green) to indicate blood vessels of the primary vascular plexus. Scale bar = 400µm. (**D**) The vascular plexus was quantified using AngioTool on vessel outgrowth, endpoints and lacunarity in mouse retinas from saline-treated SMA, PMO25-treated SMA and healthy littermate control mice. Scale bar = 400µm. One way ANOVA with Tukey post-hoc test was used for data analyse. Data represent mean ± SEM, with individual data points displayed. N≥3 eyes from ≥3 mice for each group. * $P < 0.05$, ** $P < 0.01$ *** $P < 0.001$, **** $P < 0.0001$. Scale bar = 400µm in low power images and 200µm in high power inset images. Data displayed as individual data points and mean ± SEM bars, from ≥3 eyes from ≥3 mice for each group. One way ANOVA with Tukey post hoc test. * $P < 0.05$, ** $P < 0.01$, *** $P < 0.001$.

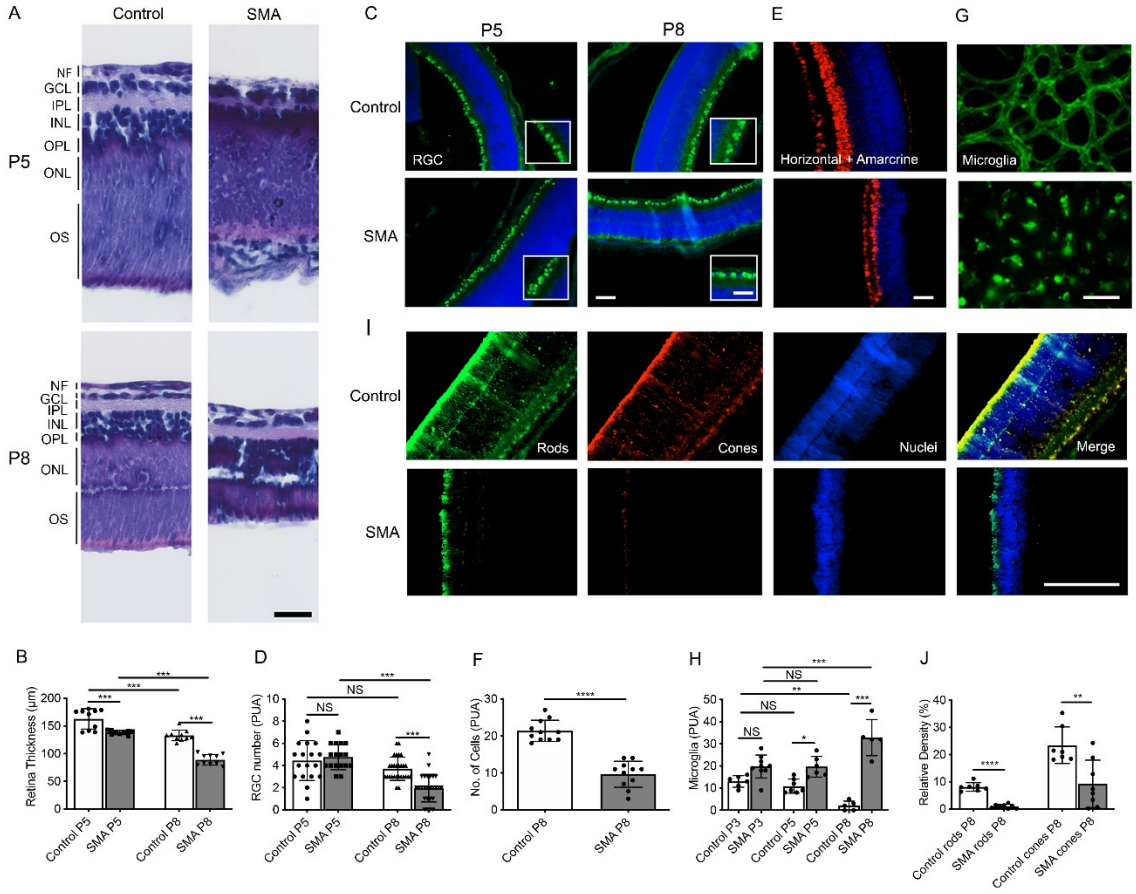

Figure 4 Depletion of neuronal components and increased microgliosis in SMA mouse retina

(**A**) Gross appearance of H&E-stained retina from SMA and healthy control mice at P5 and P8. (NF = nerve fibre, GCL = ganglion cell layer, IPL = inner plexiform layer, INL = inner nuclear layer, OPL = outer plexiform layer, ONL = outer nuclear layer, OS = outer segment). (**B**) Quantification of retinal thickness in sections from H&E staining. (**C**) Retinal ganglion cells (RGCs) stained with BRN3a (green), with nuclei in blue. The insets show high power fields of the RGC layer. (**D**) Quantification of RGCs per unit area (PUA) at P5 and P8. (**E**) Horizontal and amacrine cells were stained with PAX6 transcription factor (red), with nuclei in blue. (**F**) Quantification of horizontal and amacrine cells PUA at P8. (**G**) Microglia, stained with GSL I/ IB4 isolectin, differentiated from blood vessels by their morphology. Images were taken from the retinal periphery at P8. (**H**) Quantification of microglia cells PUA at P5 and P8. (**I**) Light sensitive photoreceptors: red/ green and blue opsin identified rods (green), rhodopsin identified cones (red), with nuclei in blue. (**J**) Relative quantification of rods and cones signals at P8. All representative images were taken at P8, except where indicated at P5. Scale bars: **A** = 100µm; **C** = 50µm for the low power images and =25µm for the high power inset images; **E** = 25µm; **G** = 50µm; **I** = 25µm. **B**, **D** and **H** were analysed by one way ANOVA with Tukey post-hoc test, **F** and **J** were analysed by unpaired two-tailed Student's T-test. The field of view (area) for assessment of cell density was 6250µm^2. Data represent mean ± SEM, with individual data points displayed. N⩾3 eyes from ⩾3 mice for each group. * P < 0.05, ** P < 0.01 *** P <0.001, **** P <0.0001.

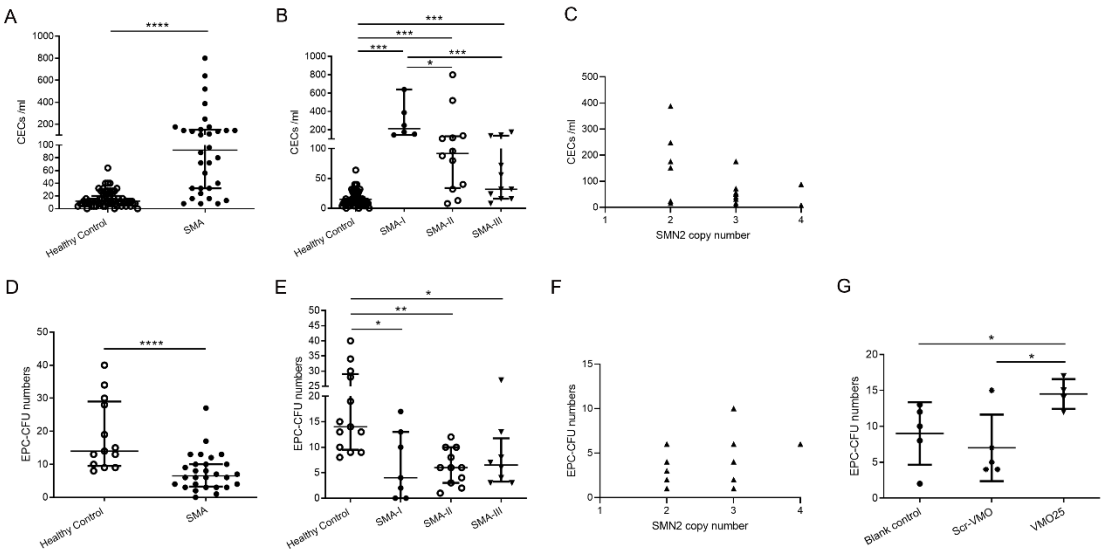

964

965 **Figure 5 Increased vascular injury and decreased vascular repair revealed in**
966 **peripheral blood from SMA patients**

967 (**A**) The levels of CECs (number/ml) in peripheral blood from SMA patients (including type
968 1, 2 and 3, n=32) and healthy control (n=17). (**B**) The comparison of CECs counts between
969 healthy control (n=17), and SMA Type 1 (n=6), Type 2 (n=12) and Type 3 (n=11). (**C**) The
970 correlation between CECs counts with the copy number of *SMN2* gene in SMA patients (r^2 =
971 0.2344, P<0.05). (**D**) The comparison of EPC-CFU numbers in peripheral blood from SMA
972 patients (including Type 1, 2 and 3, n=28) and healthy controls (n=13). (**E**) The comparison
973 of EPC-CFU numbers between healthy control and SMA Type 1 (n=7), Type 2 (n=11) and
974 Type 3 (n=8). (**F**) The correlation between numbers of EPC-CFU and *SMN2* copy (r^2 =
975 0.1696, P=0.1435). (**G**) The comparison of numbers of EPC-CFU from healthy control
976 (n=13), SMA Type 1 patients (SMA-I, n=5), EPC isolated from SMA Type 1 and treated
977 with scrambled vivo-morpholino (SMA-I+Scr-VMO, n=5) and EPC isolated from SMA Type
978 1 and treated with therapeutic AON (SMA-I+VMO25, n=5). **A** and **D** were analysed by
979 unpaired two-tailed Student's T-test, **B, E** and **G** were analysed by one way ANOVA with
980 Tukey post hoc test. **C** and **F** were analysed by Spearman rank correlation coefficient for
981 associations between CECs and EPCs with *SMN2* copy numbers. Data represent mean ±
982 SEM. * P< 0.05, **P<0.01, *** P<0.001, **** P<0.0001.

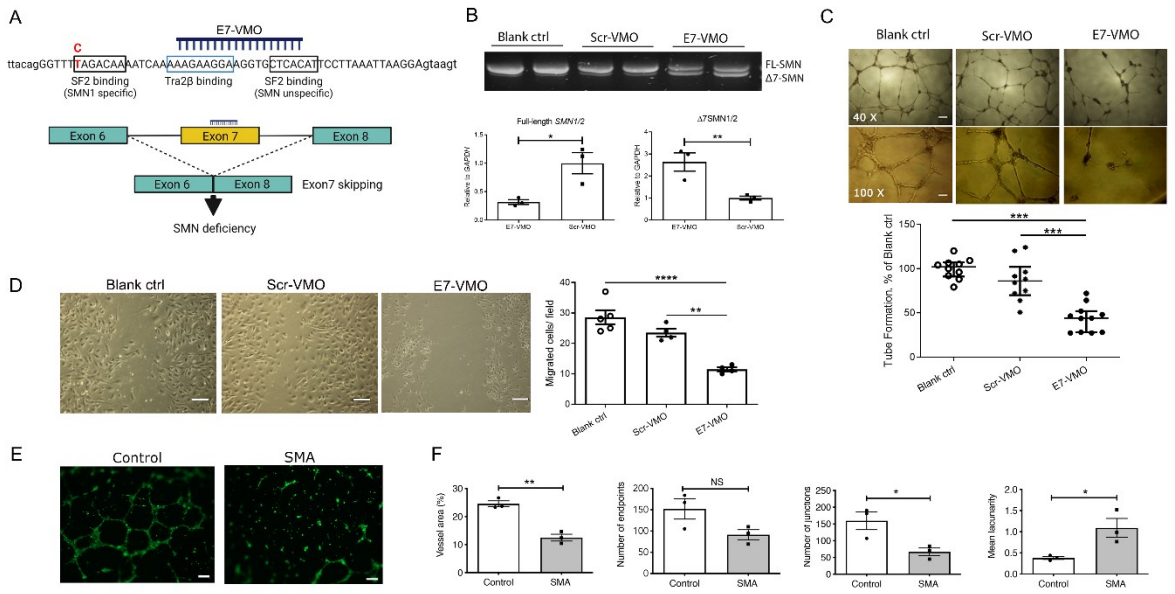

983

984 **Figure 6 Defects in angiogenesis in cultured human endothelial cells with induced**
985 **SMN deficiency**

986 (**A**) AON was designed to target exon 7 in *SMN1* and *SMN2* genes to induce exon 7 skipping.
987 (**B**) HUVECs were treated with exon 7-skipping vivo-morpholino (E7-VMO) or scrambled
988 vivo morpholino (Scr-VMO) and compared to untreated HUVECs (Blank ctrl). The *SMN1*
989 and *SMN2* exon 7 skipped by AONs was measured by reverse transcript PCR and
990 quantitative RT-PCR, respectively. Data were analysed by unpaired two-tailed Student's T
991 test. (**C**) Vascular tube formation in untreated HUVECs (blank control, n=10), HUVECs
992 treated with Scr-VMO (n=10) or E7-VMO (n=11). Images were captured at objective of 40×
993 and 100×, respectively. Tube formation was quantified as percentage to blank control. Scale
994 bars: 100µm in 40× and 200µm in 100× images. Data were analysed by one way ANOVA
995 and Tukey post hoc test. (**D**) The endothelial cells migration in HUVECs of blank control,
996 and cells treated with Scr-VMO and E7-VMO. HUVEC migration was quantified and
997 analysed by one way ANOVA and Tukey post hoc test. Scale bar = 200µm. (**E**) The cultured
998 endothelial networks from endothelial cells isolated from aortas harvested from SMA mice
999 and healthy controls at P4-6, visualised after calcein dye uptake. Scale bar = 200µm. (**F**).
1000 Parameters on endothelial networks were analysed by AngioTool. Data were analysed by
1001 unpaired two-tailed Student's T-test. Data represent mean ± SEM, with individual data points
1002 displayed. * P<0.05, ** P< 0.01, *** P<0.001.

Table 1. Retinal imaging fractal dimension

Method	Region of Interest	Patients Mean (SD) N = 21 (L = 10) (R = 11)	Controls Mean (SD) N = 46 (L = 23) (R = 23)	*Patients vs Controls* β (95% CI)	p-value
Pellegrini et al (34) AUC = 0.97	**Standardised**	1.402 (.020) [0]	1.422 (.015) [2]	-0.019 (-.028 to .009)	**<.001**
	Posterior disc	1.382 (.032) [2]	1.390 (.033) [0]	-0.016 (-.037 to .005)	.180
	Midperiphery	1.308 (.034) [1]	1.321 (.024) [2]	-0.019 (-.037 to .002)	.010
IterNet (33) AUC = 0.98	**Standardised**	1.477(.020) [0]	1.492 (.009) [2]	-0.017 (-.028 to .007)	**.001**
	Posterior disc	1.443 (.019) [0]	1.492 (.009) [4]	-0.018 (-.027 to .009)	**<.001**
	Midperiphery	1.387 (.033) [0]	1.398 (.020) [1]	-0.014 (-.029 to .003)	.190

Table caption: The FD values mean and (SD) for SMA patients and controls are tabulated for each ROI for two different techniques of segmentation, Pellegrini *et al* 2014 (34) and IterNEt 2020 (33). FD values for SMA patients were significantly lower in the standardised ROI indicating a less complex pattern of retinal branching than controls. AUC = Area under the curve.